

On the Feedback of Ice–Ocean Stress Coupling from Geostrophic Currents in an Anticyclonic Wind Regime over the Beaufort Gyre

QIANG WANG

Alfred-Wegener-Institut Helmholtz-Zentrum für Polar- und Meeresforschung, Bremerhaven, Germany, and Laboratory for Regional Oceanography and Numerical Modeling, Qingdao National Laboratory for Marine Science and Technology, Qingdao, China

JOHN MARSHALL, JEFFERY SCOTT, AND GIANLUCA MENEGHELLO

Department of Earth, Atmospheric and Planetary Sciences, Massachusetts Institute of Technology, Cambridge, Massachusetts

SERGEY DANILOV AND THOMAS JUNG

Alfred-Wegener-Institut Helmholtz-Zentrum für Polar- und Meeresforschung, Bremerhaven, and Department of Mathematics and Logistics, Jacobs University, and Institute of Environmental Physics, University of Bremen, Bremen, Germany

(Manuscript received 7 September 2018, in final form 20 November 2018)

ABSTRACT

Based on analysis of observational data it has been suggested that a negative feedback of ice–ocean stress coupling may limit freshwater accumulation in the Beaufort Gyre (BG). In this paper we explore how this feedback can significantly contribute to BG stabilization in an anticyclonic wind regime. We use an ice–ocean model and turn on and off the feedback in simulations to elucidate the role of the feedback. When a persistent anticyclonic wind anomaly is applied over the BG, liquid freshwater content (FWC) increases because of enhanced Ekman downwelling. As a consequence, ocean surface geostrophic currents speed up. However, the spinup of sea ice is weaker than the acceleration of surface geostrophic currents during wintertime, because of strong sea ice internal stress when ice concentration is high and ice is thick. This leads to cyclonic anomalies in the ice–ocean relative velocity and stress over the BG. The resultant seasonal Ekman upwelling anomaly reduces freshwater accumulation by about 1/4 as compared to a simulation with the negative feedback turned off in a control experiment, with a reduction range of 1/10–1/3 in all experiments conducted. We show that the feedback is more effective when the model’s mesoscale eddy diffusivity is smaller or when sea ice internal stress is stronger. Finally, we argue that the ice–ocean stress feedback may become less significant as the Arctic warms and sea ice declines.

1. Introduction

The Beaufort Gyre (BG) is the largest freshwater reservoir of the Arctic Ocean. Because of the potential

impact of the Arctic freshwater on the large-scale ocean circulation and climate (Aagaard et al. 1985), understanding the freshwater dynamics of the BG region has drawn much attention in the scientific community (see the review by Proshutinsky et al. 2015).

Freshwater accumulation in the BG is driven by the anticyclonic wind associated with the high atmospheric pressure over this region. Hence, variations of BG liquid freshwater content (FWC) are correlated with changes in atmospheric circulation regimes (Proshutinsky et al. 2002, 2009). The accumulation of freshwater by the wind-driven Ekman convergence and downwelling is counteracted by mesoscale eddy transport, and the

Denotes content that is immediately available upon publication as open access.

Supplemental information related to this paper is available at the Journals Online website: <https://doi.org/10.1175/JPO-D-18-0185.s1>.

Corresponding author: Qiang Wang, Qiang.Wang@awi.de

DOI: 10.1175/JPO-D-18-0185.1

© 2019 American Meteorological Society. For information regarding reuse of this content and general copyright information, consult the [AMS Copyright Policy \(www.ametsoc.org/PUBSReuseLicenses\)](https://www.ametsoc.org/PUBSReuseLicenses).

balance of these two effects is thought to act to maintain the level of freshwater storage in the gyre (Davis et al. 2014; Lique et al. 2015; Manucharyan and Spall 2016; Yang et al. 2016). Changes in freshwater sources (river runoff, precipitation, glacial and sea ice meltwater, and Pacific Water) and in freshwater circulation pathways modulated by wind forcing also contribute to changes in the FWC in the Canadian basin and BG region (Krishfield et al. 2014; Morison et al. 2012; Yamamoto-Kawai et al. 2009).

The FWC in the BG has increased dramatically during the last two decades when the atmospheric circulation was predominantly in an anticyclonic regime (Giles et al. 2012; Proshutinsky et al. 2015; Rabe et al. 2011; Zhang et al. 2016), along with enhanced mesoscale eddy activity (Zhao et al. 2016). Spatial redistribution of meteoric water toward the western Arctic can explain part of the FWC increase in the Canada basin as revealed by observations (Alkire et al. 2017). It is found that rapid Arctic sea ice decline contributed to about half of the freshwater accumulated in the BG in the 2000s by increasing freshwater available to the BG (Wang et al. 2018a). Satellite observations of sea surface height (SSH) indicate that the anticyclonic geostrophic currents in the BG have become stronger following the accumulation of freshwater since the last decade (Armitage et al. 2016, 2017). Contemporaneously, sea ice speeds in the BG region have trended upward (Spren et al. 2011; Petty et al. 2016).

Recent studies suggest that the response of freshwater storage to wind forcing can be mediated by sea ice internal stress (Kwok and Morison 2017; Dewey et al. 2018; Zhong et al. 2018; Meneghello et al. 2018a). Kwok and Morison (2017) discussed the importance of sea ice internal stress in a case when wind forcing changes. On average both sea ice and surface currents move in an anticyclonic sense under the influence of the anticyclonic winds of the Beaufort high. When the winds over the BG weaken, sea ice is slowed to below ocean surface velocity by ice internal stress. Ice–ocean stress on the ocean surface then becomes cyclonic, leading to Ekman upwelling and freshwater release. They speculate that an opposite process occurs if the winds become stronger. This interaction between ocean geostrophic currents and sea ice was analyzed from an observational point of view by Meneghello et al. (2017) in the context of estimating the BG eddy intensity. Based on observed surface geostrophic currents and sea ice drift, Dewey et al. (2018) suggest that the BG shifted to a state in which the ocean has stronger geostrophic currents that can drive the ice from below in the absence of high winds. The resultant cyclonic ocean surface stress and Ekman upwelling act to limit the increase of freshwater and

stabilize the BG (Dewey et al. 2018; Zhong et al. 2018). Recent observations also reveal a clear seasonal cycle in Ekman pumping over the BG, with intense downwelling in autumn and upwelling in winter, despite the wind forcing being downwelling favorable all year-round (Meneghello et al. 2018b). The impact of increasing surface geostrophic velocity on ice–ocean stress, that is, the negative feedback of ice–ocean stress coupling, is dubbed the “ice–ocean governor” by Meneghello et al. (2018a).

In this study we explore the role of the ice–ocean stress feedback in limiting freshwater accumulation in the BG when the BG is in an anticyclonic wind regime, as in the recent period starting from the mid-2000s. The schema shown in Figs. 1a,b presents the key elements. In the presence of an anticyclonic wind anomaly, Ekman convergence and downwelling increase. Because of the presence of lateral stresses internal to the ice, which increase exponentially with ice concentration, Ekman convergence has a pronounced seasonal variation, being stronger in warmer months. The BG accumulates freshwater, and ocean surface geostrophic currents strengthen following the doming of SSH. However, the speedup of the sea ice is expected to be weaker than the ocean in cold seasons when sea ice concentration and ice thickness, and thus ice internal stresses, are large. Thus, enhanced anticyclonic ocean currents will rub up against the sea ice resulting in upwelling anomalies, providing a negative feedback on freshwater accumulation. The feedback process described above is summarized in the following.

- 1) The FWC in the BG increases in the presence of an anticyclonic wind forcing anomaly, because of enhanced ocean surface anticyclonic stress and thus Ekman downwelling.
- 2) The SSH increases with the freshening of the gyre, which results in stronger anticyclonic ocean surface geostrophic currents.
- 3) Sea ice spins up, too. It accelerates more than the ocean when ice concentration and thickness, and thus lateral internal stresses, are low (in warm months, Fig. 1a). However, the increase in ice speed is diminished when ice concentration and thickness, and thus lateral internal stresses, are high (in cold months, Fig. 1b).
- 4) In the latter condition, the resulting anomaly of ocean surface stress is cyclonic relative to the case when the ocean surface geostrophic velocity is assumed not to increase (cf. Figs. 1b and 1d).
- 5) This leads to an Ekman upwelling anomaly, which diminishes freshwater accumulation.

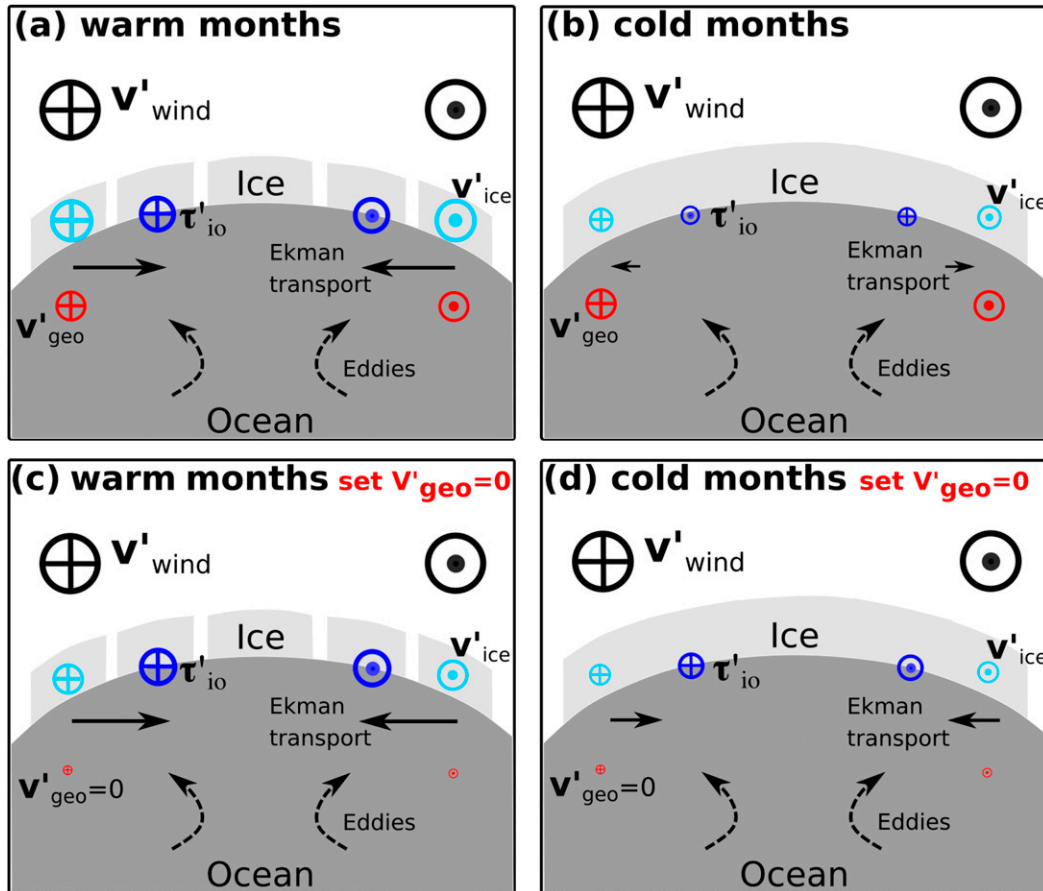


FIG. 1. Schematic diagrams illustrating the negative feedback of ice–ocean stress made possible by lateral stresses internal to the ice. The diagrams pertain to a scenario in which an anticyclonic wind anomaly acts over the BG. Vectors of wind, ice and ocean velocity, and ice–ocean stress indicate anomalies. The anticyclonic wind anomaly leads to an increase in the freshwater content, doming of the sea surface height, and enhancement of the anticyclonic geostrophic current. (a) The Ekman downwelling is stronger when ice concentration and thickness, and hence lateral internal stresses, are low as shown. (b) The speedup of sea ice under the anticyclonic wind anomaly is smaller than geostrophic currents when stresses internal to the ice are high. This leads to a cyclonic ice–ocean stress anomaly, thus Ekman divergence and upwelling anomaly. (c),(d) To understand what will happen if the feedback from geostrophic currents is not present, we carried out simulations in which the changes in currents are not taken into account in the computation of the ice–ocean stress. The difference between the case of (a) and (b) and the case of (c) and (d) reveals the feedback due to the interaction of geostrophic currents with the sea ice above. This figure is adapted from Kwok and Morison (2017) and Dewey et al. (2018) to explain the effect of the ice–ocean stress feedback associated with the seasonality of sea ice internal stress in a case of persistent anticyclonic wind forcing.

In summary, our hypothesis is the following: ice–ocean stress feedback limits the accumulation of freshwater in the BG, even when winds are in a *persistent* anticyclonic regime. In previous studies, ice–ocean stress and Ekman pumping velocity in the BG were calculated using observed geostrophic velocity and sea ice drift speed, which allows one to quantify the effect of taking ocean geostrophic currents into account in the stress calculation (Dewey et al. 2018; Meneghello et al. 2018b; Zhong et al. 2018). In this paper we will use numerical simulations to explore the idea in a controlled setting using a global ice–ocean model. In the

simulations we eliminate the contribution of ocean currents interacting with the ice by turning off changes in geostrophic velocity in the calculation of ice–ocean stress (see the model description section for details). In this way we can explore how Ekman pumping rates and freshwater accumulation will change if the feedback of geostrophic currents does not exist (i.e., if the ice–ocean stress does not see the increase of geostrophic velocity) by comparing the situations in Figs. 1a and 1b and Figs. 1c and 1d.

Our paper is ordered as follows. In section 2 we describe the model and experimental methods. The results

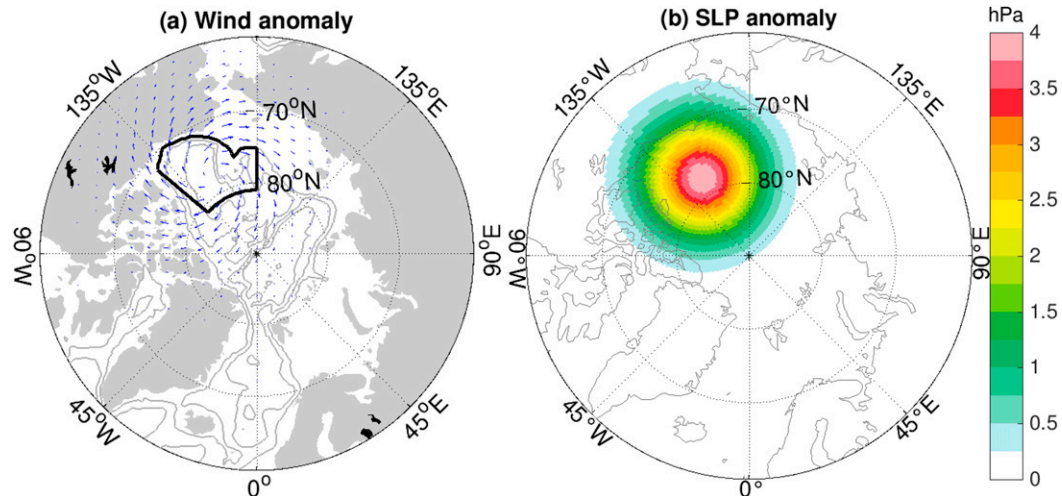


FIG. 2. (a) The wind anomaly used in the sensitivity simulations of the reference experiment and (b) the associated sea level pressure (SLP) anomaly. The defined BG region is indicated by the black box in (a).

are presented in section 3. Discussion and conclusions are provided in sections 4 and 5, respectively.

2. Model description

We use the Finite Element Sea Ice-Ocean Model (FESOM; Wang et al. 2014). FESOM is a multi-resolution ocean general circulation model based on an unstructured-mesh method (Danilov et al. 2004; Wang et al. 2008). We apply a global setup at a nominal 1° horizontal resolution in most parts of the ocean and 24 km north of 45°N . The resolution is also refined along the coast and in the equatorial band. In the vertical, 47 z levels are used with 10-m resolution in the upper 100-m depth. This mesh has been used in previous model intercomparison studies on the Arctic Ocean liquid and solid freshwater budget and content (Wang et al. 2016b,c).

The sea ice component of the model applies the elastic-viscous-plastic rheology (EVP; Hunke 2001) and thermodynamics following Parkinson and Washington (1979). Sea ice is discretized on the same unstructured mesh as the ocean, allowing direct field and flux exchanges between the two components, which are coupled through heat and water fluxes and ocean–ice stress. A modified version of EVP is used in FESOM to speed up the convergence of the sea ice solver (Danilov et al. 2015), which allows one to reproduce observed statistics of sea ice leads and linear kinematic features given acceptable model resolution (Wang et al. 2016a). Previous studies have shown that FESOM can faithfully represent Arctic sea ice concentration and thickness when compared to observations and other models (e.g., Wekerle et al. 2013; Wang et al. 2016b, 2018b).

The ocean is initialized with temperature and salinity from the Polar Science Center Hydrographic Climatology version 3 (Steele et al. 2001) with the currents set to zero, and sea ice is initialized with a field obtained from a previous simulation. A control simulation forced by the repeating normal year atmospheric dataset (Large and Yeager 2009) is carried out for 60 years. The normal year forcing represents the mean climatology of atmospheric fields and fluxes (1984–2000). It consists of one year of forcing fields at 6-hourly intervals of near-surface winds, air temperature and humidity, daily downward longwave and shortwave radiation, and monthly precipitation. The monthly river runoff climatology provided by Dai et al. (2009) is used.

Branching out from the thirtieth year of the control run, one sensitivity simulation (named as “BGplus”) is made following the protocol of BG wind anomaly experiments described by Marshall et al. (2017). A constant-in-time anticyclonic wind anomaly centered over the BG is added to the wind forcing (Fig. 2), and the simulation is continued for 30 years. Justification of the chosen wind anomaly magnitude, in the context of the region’s internal variability, is discussed in Marshall et al. (2017); the resulting increase in FWC due to this anomaly is of similar order of magnitude as the observed FWC change in the 2000s (Proshutinsky et al. 2015).

We carried out another calculation, which is the same as BGplus except that we modify the geostrophic velocity in the calculation of the ice–ocean stress

$$\boldsymbol{\tau}_{io} = \rho C_{io} |\mathbf{v}_{ice} - \mathbf{v}_{oce}| (\mathbf{v}_{ice} - \mathbf{v}_{oce}),$$

where ρ is ocean density; $C_{io} = 5.5 \times 10^{-3}$ is the ice–ocean drag coefficient; and \mathbf{v}_{ice} and \mathbf{v}_{oce} are sea ice and

TABLE 1. List of experiments showing differences in model setups. In each of the experiments three simulations (control, BGplus, and BGplus/noGeo) are carried out.

Experiments	Reference	Wind/2	GM3	GM/2	P/2
SLP anomaly magnitude	4 hPa	2 hPa	4 hPa	4 hPa	4 hPa
GM eddy diffusivity	$500 \text{ m}^2 \text{ s}^{-1}$	$500 \text{ m}^2 \text{ s}^{-1}$	$1500 \text{ m}^2 \text{ s}^{-1}$	$250 \text{ m}^2 \text{ s}^{-1}$	$500 \text{ m}^2 \text{ s}^{-1}$
Ice strength parameter P^*	$27\,500 \text{ N m}^{-2}$	$27\,500 \text{ N m}^{-2}$	$27\,500 \text{ N m}^{-2}$	$27\,500 \text{ N m}^{-2}$	$13\,750 \text{ N m}^{-2}$

ocean surface velocities, respectively. In this sensitivity simulation the ocean surface velocity in the ice–ocean stress calculation is modified thus: $u_{\text{occ}}^* = u_{\text{occ}} - g/f\partial_y(\eta_{\text{control}} - \eta)$ and $v_{\text{occ}}^* = v_{\text{occ}} + g/f\partial_x(\eta_{\text{control}} - \eta)$, where η is the SSH simulated at the current model time step, g is the gravity acceleration, f is the Coriolis parameter, and η_{control} is the daily mean SSH saved from the control run. By modifying the calculation of the stress we intentionally eliminate the feedback from geostrophic currents in the sea ice–ocean coupling. Hereafter, this simulation is called “BGplus/noGeo.”

In BGplus/noGeo we use *daily* mean SSH saved from the control run, instead of SSH saved from every model time step, given storage limitations. To demonstrate that daily mean SSH is sufficient, we repeated the control run with the modified stress computation as described above; we found that the model result is essentially indistinguishable from the control run.

The three simulations described above are referred to as the “reference” experiment. Another four sets of experiments are conducted to assess robustness of the feedback to varying wind anomaly strength and key model parameters (called wind/2, GM3, GM/2, and P/2, respectively, see Table 1). In experiment wind/2, we reduce the magnitude of the anticyclonic wind anomaly to half of that used in the reference experiment. This experiment allows us to investigate the feedback in the case of smaller wind perturbation.

The eddy GM diffusivity (Gent and McWilliams 1990) is set to $500 \text{ m}^2 \text{ s}^{-1}$ in the reference experiment. This is broadly in accord with the values inferred from observations presented in Meneghello et al. (2017). There, mixing length theory was applied to BG mooring data to show that eddy diffusivity decreases from more than $1000 \text{ m}^2 \text{ s}^{-1}$ in the near surface of the BG to about $100\text{--}300 \text{ m}^2 \text{ s}^{-1}$ in the deeper ocean. Guided by this range we change the GM diffusivity to 1500 and $250 \text{ m}^2 \text{ s}^{-1}$ in experiments GM3 and GM/2, respectively. These two experiments will demonstrate how the feedback responds to the strength of parameterized eddy activity.

Experiment P/2 is designed to explore sensitivity to the sea ice strength parameter P^* . We reduce P^* from $27\,500 \text{ N m}^{-2}$ [the value suggested by Hibler and Walsh (1982)] in the reference experiment to $13\,750 \text{ N m}^{-2}$

in experiment P/2. Sea ice strength is proportional to $P = P^*h \exp[-C(1-a)]$, where h is sea ice thickness, $C = 20$, and a is the sea ice concentration. This experiment, then, represents a condition in which the sea ice is weaker. Although we change the sea ice strength by reducing P^* , the experiment can also provide information on the response of the stress feedback to sea ice weakening (smaller P) induced by reduction in sea ice concentration or thickness in a warmer climate.

In each experiment we carry out three simulations: a 60-yr control run, a 30-yr BGplus run, and a 30-yr BGplus/noGeo run. In total, 14 simulations are conducted and analyzed.

3. Results

a. Reference experiment

In the control run of the reference experiment, the liquid FWC (calculated using a reference salinity of 34.8 and integrated from the surface to the depth of the reference salinity) in the BG is at equilibrium during the last 30 years (see Fig. S1a in the online supplemental material). The seasonal oscillation in FWC is due to the seasonal variation of both freshwater availability and Ekman pumping. After adding the anticyclonic wind anomaly, the FWC increases with time in the BGplus simulation (Fig. S1a and Fig. 3a); see also Marshall et al. (2017), where the similar experimental result is discussed at length in the context of *climate response functions*. The inflation rate of the FWC starts to saturate with time, as expected from the counteracting effects of eddies. When the feedback of ice–ocean stress is eliminated (the simulation BGplus/noGeo), the increase of the FWC induced by the same wind anomaly is larger, suggesting that geostrophic currents play an important role.

The accumulation of liquid freshwater in the BG under the anticyclonic wind anomaly is consistent with enhanced Ekman downwelling (Fig. 3b). The feedback of ice–ocean stress reduces the Ekman downwelling, and thus the freshwater accumulation (Figs. 3a,b). The most rapid changes in Ekman pumping take place during the first 2–3 years of the simulation BGplus (Fig. 3b). The feedback of ice–ocean stress reduces the annual mean Ekman downwelling and the accumulation of freshwater by 46% and 23%, respectively, at the end of the simulation.

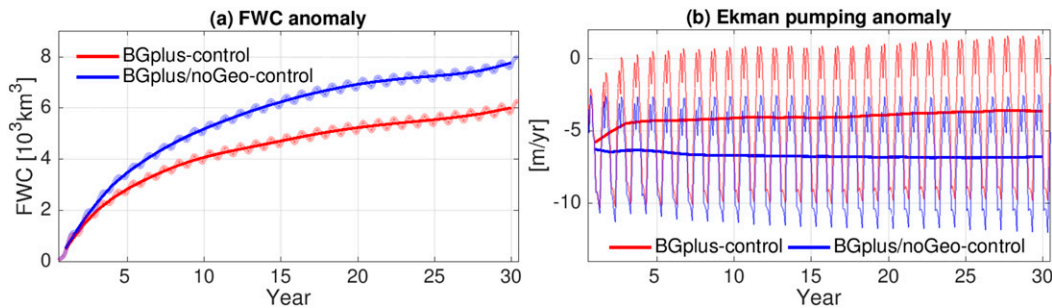


FIG. 3. (a) The anomaly in BG liquid FWC in the BGplus and BGplus/noGeo experiments referenced to the control run. (b) The anomaly of BG Ekman pumping referenced to the control run. Annual means are shown together with monthly means. All results shown are for the “reference” experiments.

To better illustrate the seasonal variability and temporal evolution of the Ekman pumping, we show the monthly mean difference between the wind anomaly runs and the control run over three different periods in Figs. 4a–c. In the first year, when geostrophic currents have not yet changed much, the impact of the anticyclonic wind anomaly on Ekman pumping is very similar in the two sensitivity runs. The Ekman downwelling is enhanced in all seasons, although the impact is much smaller in winter when the BG is almost fully covered by sea ice (Figs. 4a and 4e). After several years, Ekman downwelling changes only marginally in simulation BGplus/noGeo, whereas a significant reduction in the Ekman downwelling takes place from November to the following June in simulation BGplus (Figs. 4b,c). In fact, during some winter months, the anticyclonic wind anomaly even leads to a positive Ekman pumping anomaly (i.e., reducing the Ekman downwelling) after a few years into the simulation BGplus (Figs. 4b,c). As a consequence of this seasonality, the difference of the Ekman pumping between the two sensitivity runs shows a clear annual cycle (Fig. 4d).

The stress between the sea ice and ocean is determined by their relative velocity. The differences between BGplus and BGplus/noGeo in sea ice speed (Fig. 5d) and ocean surface speed (the one used in the calculation of the stress, Fig. 6d) reveal that the seasonal variation of the Ekman pumping difference is mainly due to sea ice speed differences. Indeed, when the feedback of ice–ocean stress is eliminated in BGplus/noGeo, both the sea ice speed and ocean surface speed (the one used in the calculation of the stress) do not show significant changes during the 30 years simulation (Figs. 5a,b,c and 6a,b,c). In contrast, in simulation BGplus, the ocean surface speed increases in all seasons following the increase of the liquid FWC and SSH with time, while the sea ice speed increases much less significantly when sea ice concentration is high (close to be 100%). The latter occurs because in this case the sea ice

internal stress, which strongly depends on the sea ice concentration, is the predominant factor controlling the sea ice momentum balance. Therefore, our results suggest that the ice–ocean stress feedback is more effective when sea ice concentration is very high (cf. Figs. 4d and 4e). Our simulations also imply that the speedup of sea ice drift in the BG region observed by satellites can be partly attributed to the increase of the ocean surface geostrophic velocity (Figs. 5a,b). This effect is present in all seasons but is less pronounced in winter.

b. Sensitivity experiments

Similar to the reference experiment, the imposed anticyclonic wind anomaly enhances Ekman downwelling in the BGplus setups of all sensitivity experiments (Fig. 7a). Moreover, all the BGplus simulations show that the Ekman downwelling weakens during the first few years, when the liquid FWC increases rapidly (cf. Figs. 7a and 8a). In all simulations in which the ice–ocean stress feedback is eliminated (BGplus/noGeo), the Ekman downwelling, in contrast, does not show rapid initial weakening (Fig. 7c), and is stronger than in their BGplus counterparts (Fig. 7e). The experiments consistently show that the wind anomaly enhances the Ekman downwelling most significantly in summer (Figs. 7b,d), while the effect of the feedback on Ekman pumping is the strongest in winter (Fig. 7f).

When the magnitude of the wind anomaly is reduced (comparing experiments wind/2 and reference), the strength of the Ekman downwelling anomaly is reduced in all months in simulations BGplus/noGeo (Fig. 7d). However, when the feedback is included, the Ekman downwelling anomalies in the winter months do not change much between the wind/2 and reference experiments (Fig. 7b). This is because a weaker wind anomaly leads to less freshwater accumulation (Fig. 8a), and thus a weaker impact on the Ekman pumping from the feedback of ice–ocean stress (Fig. 7f). The feedback reduces the accumulated freshwater by 24% at the end

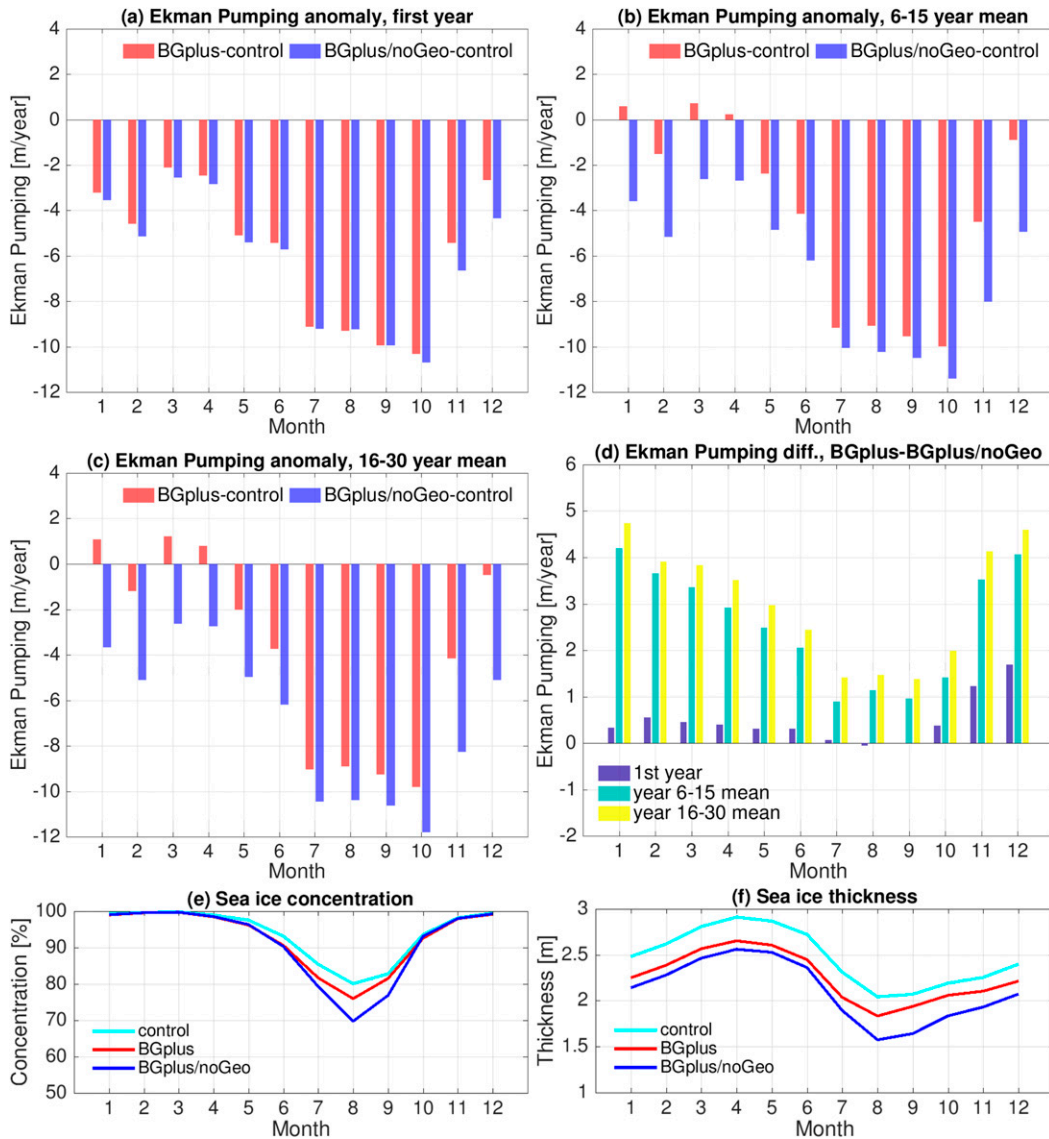


FIG. 4. The anomaly in Ekman pumping rates averaged over the BG referenced to the control run: (a) in the first year, (b) averaged from years 6 to 15, and (c) averaged from years 16 to 30. (d) The difference of the BG Ekman pumping between BGplus/noGeo and BGplus. (e) Mean BG sea ice concentration averaged from years 16 to 30. (f) As in (e), but for sea ice thickness. The results are for the reference experiment.

of the simulation in wind/2, similar to the reference experiment. In wind/2, the reduction of freshwater accumulation is smaller than in the reference experiment, while the total freshwater accumulation induced by the weaker wind is also smaller, so their ratio is not very different to the case of the reference experiment.

The Ekman pumping anomaly induced by the wind anomaly does not change much when the eddy diffusivity is changed, provided that the ice–ocean stress feedback is eliminated (experiments GM3 and GM/2, Figs. 7c,d). In contrast, with the feedback active, the Ekman downwelling is stronger with a higher eddy

diffusivity when the BG is nearly fully covered by sea ice (Fig. 7b). This is because a higher eddy diffusivity leads to a lower FWC in the BG (Fig. 8a), weaker currents and thus a weaker constraint on Ekman downwelling from the feedback in the months when it plays a role (Fig. 7f). The experiment GM/2 indicates that the feedback plays a more significant role when the stabilization effect of eddies is small (Fig. 8).

The experiment P/2 explores the case of weaker sea ice. With the same anticyclonic wind anomaly, weaker sea ice leads to stronger Ekman downwelling when sea ice concentration is close to 100% (Fig. 7b). This results

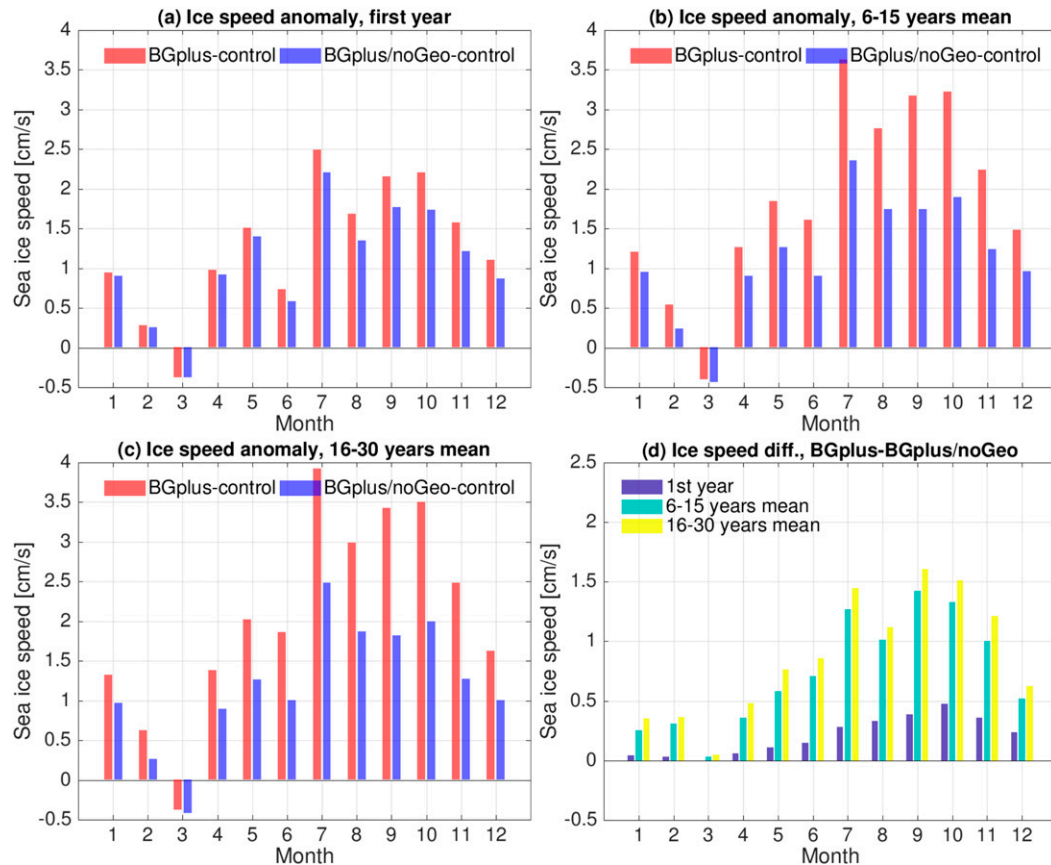


FIG. 5. The anomaly of sea ice speed over the BG referenced to the control run: (a) in the first year, (b) averaged from years 6 to 15, and (c) averaged from years 16 to 30. (d) The difference of the BG sea ice speed between BGplus/noGeo and BGplus. The results are for the reference experiment.

in enhanced freshwater accumulation (Fig. 8a). However, the effect of the ice–ocean stress feedback on Ekman pumping is weaker than in the reference experiment (Figs. 7e,f). Weaker sea ice follows more closely the increasing ocean geostrophic velocity, especially in cold seasons from autumn to early spring (Fig. S2), leading to smaller changes in the relative velocity between the sea ice and ocean and so a weaker impact of the feedback on Ekman pumping.

As a consequence of modifying Ekman pumping, the feedback acts to reduce the freshwater accumulation in the BG in all experiments (Fig. 8c). However, the impacts on the BG liquid FWC are not determined only by changes in Ekman pumping. For example, at the end of the simulations, the FWC anomaly induced by the feedback is the smallest in experiment P/2 (Fig. 8c), although the induced anomaly in Ekman pumping is not (Figs. 7e,f). Possibly, this can be explained by the fact that the total BG FWC is highest in P/2 (Fig. S3), which implies steeper isopycnal slopes and thus a stronger counteracting effect of eddies.

We find that the feedback of ice–ocean stress also influences the location of the Beaufort Gyre center. The spatial patterns of the difference in Ekman pumping velocity and FWC between different simulations are shown in Figs. S4 and S5. The feedback of ice–ocean stress reduces the Ekman downwelling in the western BG and tends to enhance it along the southern and eastern coast of the Beaufort Sea (Fig. S4). Note that the Ekman transport anomaly induced by eliminating the feedback is also directed toward the western BG (Fig. S6). Consequently the FWC anomaly induced by the feedback is centered at the western boundary of the BG (Fig. S5). Under the prescribed anticyclonic wind anomaly, the center of the gyre circulation moves toward the northwest along with the increase of FWC (Fig. S5). The feedback tends to retard the change of the centroid location. A similar finding about the impact of the feedback on freshwater spatial distribution is evident from all the experiments. Further studies are required to understand the impact of the position of the gyre and

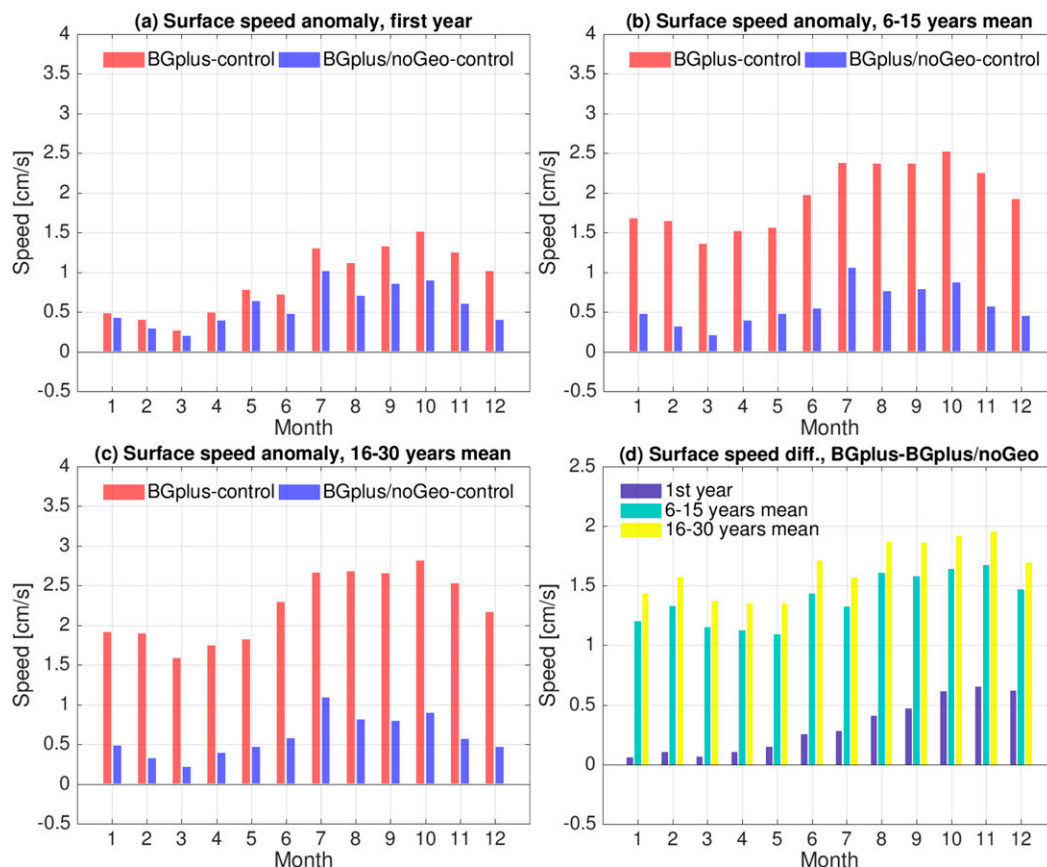


FIG. 6. The anomaly of ocean surface speed over the BG referenced to the control run: (a) in the first year, (b) averaged from years 6 to 15, and (c) averaged from years 16 to 30. (d) The difference of the BG ocean surface speed between BGplus/noGeo and BGplus. Note that the speed in BGplus/noGeo is the one that was modified in the calculation of ocean–ice stress. The results are for the reference experiment.

the availability of freshwater on the longer-term FWC response to the wind anomaly.

4. Discussion

The FWC of the BG has increased significantly over the last decade or so, a consequence of the concurrence of sea ice decline and an anticyclonic wind regime (Wang et al. 2018a). The latter is associated with the strengthening of the Beaufort high atmospheric pressure, which acts to accumulate freshwater and pump it down into the gyre. One important idea explored in, for example, Manucharyan and Spall (2016), is that the FWC is set by a balance between wind-driven Ekman downwelling tending to inflate, and mesoscale eddy transport and mixing tending to deflate the FWC. However, Meneghello et al. (2018a) argue that this idea must be significantly revised to take account of the ice–ocean governor, which regulates the Ekman pumping rate. Observational studies suggest that ocean

geostrophic currents, strengthened as a result of freshwater accumulation and SSH doming of the gyre, can impose cyclonic ice–ocean stress anomalies on the ocean when they swirl faster than the overlying sea ice drift, thus providing a negative feedback on freshwater accumulation (Kwok and Morison 2017; Dewey et al. 2018; Zhong et al. 2018; Meneghello et al. 2018a,b). Here, by using numerical simulations, we showed that this ice–ocean governor indeed acts to limit the accumulation of freshwater even in persistent, strongly anticyclonic wind regimes. The natural seasonality in ice concentration, and hence in ice internal stress, facilitates the operation of the governor.

Dewey et al. (2018) suggest that this basic feedback between the ocean and ice on weekly to monthly time scales helps to stabilize the BG to high-frequency variability. They propose that in periods of strong winds the ice drives the ocean, whereas during lulls in the wind the ocean drives the ice, leading to synoptic time-scale “curl reversals,” which act to dampen high-frequency

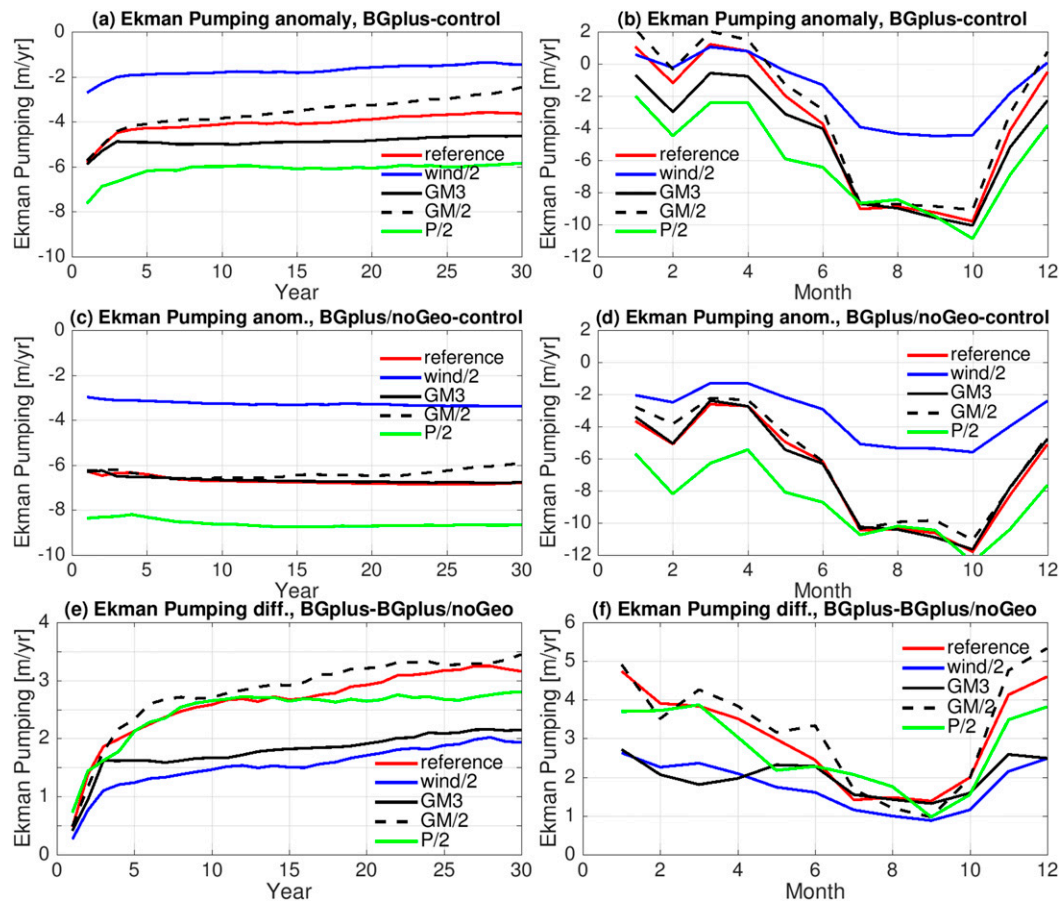


FIG. 7. The difference of the Ekman pumping rates over the BG between BGplus and the control run: (a) the time series of the annual mean and (b) the seasonal cycle averaged from years 16 to 30. (c),(d) As in (a) and (b), but for the difference between BGplus/noGeo and control. (e),(f) As in (a) and (b), but for the difference between BGplus and BGplus/noGeo.

variations. Note that in their conception, internal stress in the ice, and the relative ice–ocean velocity, play similar dynamical roles as described here, yet there is a critical difference: the focus in our study is on the decadal response to a persistent anticyclonic wind anomaly and the role that seasonality in sea ice cover plays in limiting the inflation of the gyre. Not only does thick, high-concentration sea ice coverage block momentum transfer to the ocean in winter (this is readily apparent in the simulations with the feedback effect turned off, as shown in Fig. 7d), but the rubbing of the ocean gyre against the extensive winter ice cover is a key component of the mechanism that damps the response of FWC to wind forcing. This is distinct from the response to high-frequency winds emphasized by Dewey et al. (2018). Our model results are qualitatively consistent with the seasonal variation of Ekman pumping derived from observations in recent decades (Meneghello et al. 2018b) and suggest that the ice–ocean governor

plays a critical role on the interannual-to-decadal evolution of the gyre. Future work is required to investigate how ice–ocean feedbacks operate across the full gamut of time scales—from synoptic to decadal—and their overall effect on BG FWC variability.

Through its ability to reduce Ekman downwelling, ice–ocean feedbacks significantly limit freshwater accumulation. The effect is found in all our model experiments, while the quantitative impact on FWC depends on the details of the model configurations (Fig. 8). For example, the accumulation of freshwater depends also on the counteracting eddy transport, and thus the slope of isopycnals, that is, the FWC state itself. In the experiment with lower sea ice strength (P/2), the total FWC in the BG is higher. Therefore, the FWC anomaly induced by eliminating the feedback is much smaller in this experiment than in the reference, although the anomaly of Ekman pumping is only slightly different between the two experiments. In an experiment where

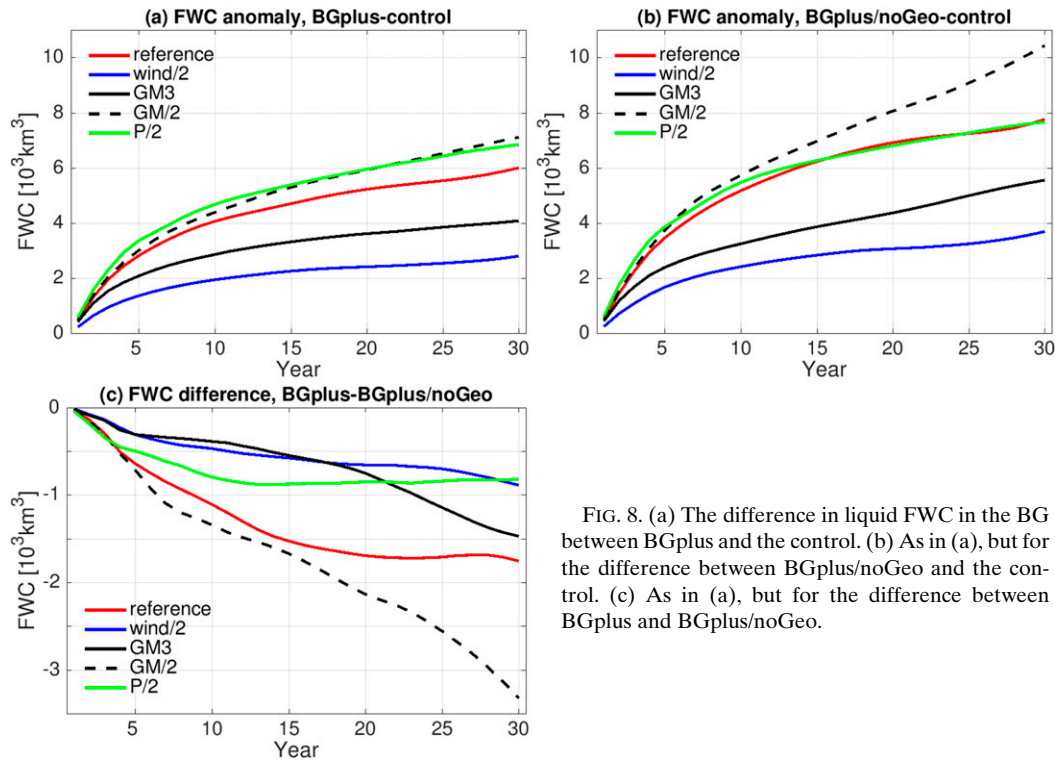


FIG. 8. (a) The difference in liquid FWC in the BG between BGplus and the control. (b) As in (a), but for the difference between BGplus/noGeo and the control. (c) As in (a), but for the difference between BGplus and BGplus/noGeo.

we decrease the size of the wind anomaly by a factor of 2 (wind/2), we find that both (i) the magnitude of the FWC response to the wind anomaly and (ii) the magnitude of the FWC anomaly induced by eliminating the feedback are about half of those in the reference run. Therefore, the efficiency of the feedback in limiting freshwater accumulation [the ratio between (i) and (ii)] is not very sensitive to the magnitude of wind anomalies in the range we explored.

Sea ice with weaker internal stress allows for an overall stronger response of the Ekman pumping to the wind forcing anomaly. First, it speeds up more significantly in response to anticyclonic winds. Second, the strength of the feedback becomes weaker (i.e., ice drift more closely follows the enhanced ocean geostrophic currents). The two factors together strengthen the Ekman downwelling in an anticyclonic wind regime. Because the feedback process is more efficient in the presence of high sea ice internal stress, it presumably will play a less important role in a warmer climate when seasons with low sea ice concentration and thickness become longer and then even winter sea ice is more mobile. One might expect not only longer seasons with enhanced downward pumping but also weaker feedback in winter months. With a less efficient governor operating, there could be significant disruption of FWC from its current state.

Applying the anticyclonic wind anomaly over the BG tends to reduce mean sea ice concentration and thickness in the BG in the reference experiment (Figs. 9a,b and 4e,f). The reduction of sea ice concentration mainly occurs in summer. The feedback from geostrophic currents hinders the reduction. Changes in sea ice concentration and volume may influence not only the total ocean surface stress, but also the surface freshwater budget. Therefore, the quantitative results obtained from the reference experiment (Fig. 3) very possibly contain some contribution from these changes. In other experiments with the same wind forcing anomaly, similar impacts of wind anomaly and ice–ocean stress feedbacks on sea ice concentration and thickness are observed. However, in the experiment with a smaller wind forcing anomaly (wind/2) the sea ice state in the BG did not change significantly (Figs. 9c,d), which represents a clean case when only the direct effect of the feedback plays a role. In this experiment the feedback of ice–ocean stress reduces the accumulation of freshwater by 1/4, a value very similar to that in the reference experiment. This certainly supports the contention that the reference run’s reduction in summer sea ice plays only a minor role. Another indication of the small contribution of the indirect impact is that the sea ice state changes slowly with time (Figs. 9a,b), while the Ekman pumping associated with the feedback changes quickly at the

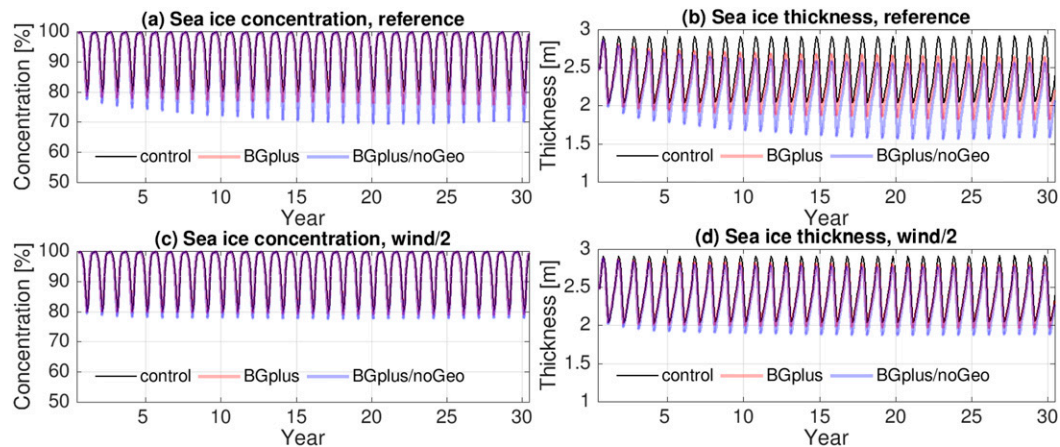


FIG. 9. Time series of sea ice (a) concentration and (b) thickness in the BG in the reference experiment. (c),(d) As in (a) and (b), but for the wind/2 experiment.

beginning of the BGplus simulation (Fig. 3b). This means that most of the Ekman pumping anomaly has little to do with the changes in sea ice state in this simulation.

The effect of the ice–ocean stress feedback is more pronounced when eddy activity is weak because the gyre is deeper and so the surface geostrophic currents stronger. In experiment GM/2 (with eddy GM diffusivity smaller than the values estimated for the upper ocean of the BG), the FWC continues to increase till the end of the simulation in the case when the feedback is turned off (Fig. 8b). The feedback significantly stabilizes the BG when it is active (Fig. 8a). The results suggest that it is crucial to resolve, or properly parameterize, meso-scale eddies to model variability of BG FWC.

The feedback significantly limits the accumulation of freshwater and reduces the time scale of gyre spinup when an anticyclonic wind forcing anomaly is imposed. However, in none of our simulations does the FWC reach a full equilibrium state after the wind forcing anomaly has been imposed for 30 years. Changing the strength of the wind forcing anomaly and eddy diffusivity affects the time scale of the gyre spinup more strongly than the effect of the feedback. The time scale of the gyre spinup depends on the realism of the eddy diffusivity. The conditions in the Arctic Ocean outside the BG and the release of freshwater to the North Atlantic may also significantly influence the time scale of the BG spinup. Future work is required to better understand various processes that influence the time scale of BG spinup.

Finally, it should be noted that BG freshwater accumulation could be amplified by increasing availability of freshwater to the BG associated with, for example, sea ice decline (Wang et al. 2018a) or enhanced river runoff and precipitation (Zhang et al. 2013; Haine et al.

2015; Carmack et al. 2016) in a warmer climate. Understanding the variability, trend, and stabilization of BG FWC demands that these factors are also taken into account.

5. Conclusions

In this study the feedback of ice–ocean stress has been explicitly illustrated using a global ice–ocean model. The feedback is associated with the presence of sea ice internal stress, which determines sea ice drift together with the stress between the ice and the underlying ocean. When winds over the BG are in an anticyclonic regime, freshwater is accumulated, leading to an increase in SSH inducing anticyclonic motion. At the same time sea ice also accelerates. However, sea ice internal stress hinders the acceleration significantly when its concentration is close to 100% and the ice is thick. This results in cyclonic ice–ocean stress and Ekman upwelling anomalies in the BG, limiting freshwater accumulation.

To quantify the effect of the feedback, we carried out simulations in which changes in geostrophic currents are eliminated in the calculation of ice–ocean stress. This method allowed us to answer what would happen to freshwater accumulation if the feedback did not exist. Our results support the hypothesis formulated in the introduction: the feedback of ice–ocean stress can limit freshwater accumulation even when winds are in a persistent anticyclonic regime. The seasonal variability of ice state allows BG FWC to increase in months with low internal ice stress as a response to the anticyclonic wind anomaly, but induces a negative feedback in months with high internal ice stress due to the spin up of the gyre (Fig. 1).

The feedback process is depicted by the schematics presented in Fig. 1 and was explored in a series of

experiments. In our reference experiment, the Ekman pumping anomaly and freshwater accumulation in the BG induced by the added wind forcing were reduced by, roughly, 1/2 and 1/4, respectively, in the presence of the feedback. Over all the cases considered, the feedback reduced the magnitude of the response to wind forcing by an order of 1/3–2/3 for Ekman pumping and 1/10–1/3 for freshwater accumulation. Our simulations indicate that the effect of the feedback is more pronounced when eddy activity is weaker. For example, when the eddy diffusivity was set to a smaller value ($250\text{ m}^2\text{ s}^{-1}$), the feedback reduced the freshwater accumulation most significantly (by 1/3). With weaker sea ice (using only one-half of the canonical sea ice strength parameter), the feedback had the least impact (reducing the freshwater accumulation by only 1/10). We suggest that in a warmer climate the feedback will possibly become less significant because of shorter seasons with high sea ice internal stress.

Use of eddy-resolving resolutions in Arctic Ocean simulations would be very helpful for better understanding the interplay between Ekman pumping, eddy transport, and the feedback associated with ice internal stress. This is currently challenging, but could soon become possible with the advancement in models and computers. Sea ice internal stress is the key element in the feedback process studied here and so a faithful representation of ice rheology is crucial if our models are to adequately represent the spinup and spindown of a partially and seasonally ice-covered gyre. In particular, sea ice rheology and ice floe size distributions could be important factors influencing simulated sea ice dynamics and thermodynamics (e.g., Dumont et al. 2011; Horvat et al. 2016; Rampal et al. 2016; Rabatel et al. 2018; Roach et al. 2018). Studies on their impact on ocean–ice interaction and BG freshwater accumulation are required in future work.

Acknowledgments. The AWI group was supported by the Helmholtz Climate Initiative REKLIM (Regional Climate Change) of Germany. The MIT group was supported by the NSF Arctic Program and by NASA through the MIT–GISS collaborative agreement. We thank the reviewers for their helpful comments. We also would like to thank Ed Doddridge for helpful discussions. The simulations were performed at the North-German Supercomputing Alliance (HLRN).

REFERENCES

- Aagaard, K., J. H. Swift, and E. Carmack, 1985: Thermohaline circulation in the Arctic Mediterranean Seas. *J. Geophys. Res.*, **90**, 4833–4846, <https://doi.org/10.1029/JC090iC03p04833>.
- Alkire, M. B., J. Morison, A. Schweiger, J. Zhang, M. Steele, C. Peralta-Ferriz, and S. Dickinson, 2017: A meteoric water budget for the Arctic Ocean. *J. Geophys. Res. Oceans*, **122**, 10 020–10 041, <https://doi.org/10.1002/2017JC012807>.
- Armitage, T., S. Bacon, A. Ridout, S. Thomas, Y. Aksenov, and D. Wingham, 2016: Arctic sea surface height variability and change from satellite radar altimetry and GRACE, 2003–2014. *J. Geophys. Res. Oceans*, **121**, 4303–4322, <https://doi.org/10.1002/2015JC011579>.
- , —, —, A. Petty, S. Wolbach, and M. Tsamados, 2017: Arctic Ocean surface geostrophic circulation 2003–2014. *Cryosphere*, **11**, 1767–1780, <https://doi.org/10.5194/tc-11-1767-2017>.
- Carmack, E. C., and Coauthors, 2016: Freshwater and its role in the Arctic Marine System: Sources, disposition, storage, export, and physical and biogeochemical consequences in the Arctic and global oceans. *J. Geophys. Res. Biogeosci.*, **121**, 675–717, <https://doi.org/10.1002/2015JG003140>.
- Dai, A., T. Qian, K. E. Trenberth, and J. D. Milliman, 2009: Changes in continental freshwater discharge from 1948 to 2004. *J. Climate*, **22**, 2773–2792, <https://doi.org/10.1175/2008JCLI2592.1>.
- Danilov, S., G. Kivman, and J. Schröter, 2004: A finite-element ocean model: Principles and evaluation. *Ocean Modell.*, **6**, 125–150, [https://doi.org/10.1016/S1463-5003\(02\)00063-X](https://doi.org/10.1016/S1463-5003(02)00063-X).
- , Q. Wang, R. Timmermann, N. Iakovlev, D. Sidorenko, M. Kimmritz, T. Jung, and J. Schroeter, 2015: Finite-Element Sea Ice Model (FESIM), version 2. *Geosci. Model Dev.*, **8**, 1747–1761, <https://doi.org/10.5194/gmd-8-1747-2015>.
- Davis, P. E. D., C. Lique, and H. L. Johnson, 2014: On the link between Arctic sea ice decline and the freshwater content of the Beaufort Gyre: Insights from a simple process model. *J. Climate*, **27**, 8170–8184, <https://doi.org/10.1175/JCLI-D-14-00090.1>.
- Dewey, S., J. Morison, R. Kwok, S. Dickinson, D. Morison, and R. Andersen, 2018: Arctic ice-ocean coupling and gyre equilibrium observed with remote sensing. *Geophys. Res. Lett.*, **45**, 1499–1508, <https://doi.org/10.1002/2017GL076229>.
- Dumont, D., A. Kohout, and L. Bertino, 2011: A wave-based model for the marginal ice zone including a floe breaking parameterization. *J. Geophys. Res.*, **116**, C04001, <https://doi.org/10.1029/2010JC006682>.
- Gent, P. R., and J. C. McWilliams, 1990: Isopycnal mixing in ocean circulation models. *J. Phys. Oceanogr.*, **20**, 150–155, [https://doi.org/10.1175/1520-0485\(1990\)020<0150:IMOCM>2.0.CO;2](https://doi.org/10.1175/1520-0485(1990)020<0150:IMOCM>2.0.CO;2).
- Giles, K. A., S. W. Laxon, A. L. Ridout, D. J. Wingham, and S. Bacon, 2012: Western Arctic Ocean freshwater storage increased by wind-driven spin-up of the Beaufort Gyre. *Nat. Geosci.*, **5**, 194–197, <https://doi.org/10.1038/ngeo1379>.
- Haine, T., and Coauthors, 2015: Arctic freshwater export: Status, mechanisms, and prospects. *Global Planet. Change*, **125**, 13–35, <https://doi.org/10.1016/j.gloplacha.2014.11.013>.
- Hibler, W., and J. Walsh, 1982: On modeling seasonal and interannual fluctuations of Arctic sea ice. *J. Phys. Oceanogr.*, **12**, 1514–1523, [https://doi.org/10.1175/1520-0485\(1982\)012<1514:OMSAIF>2.0.CO;2](https://doi.org/10.1175/1520-0485(1982)012<1514:OMSAIF>2.0.CO;2).
- Horvat, C., E. Tziperman, and J. Campin, 2016: Interaction of sea ice floe size, ocean eddies, and sea ice melting. *Geophys. Res. Lett.*, **43**, 8083–8090, <https://doi.org/10.1002/2016GL069742>.
- Hunke, E. C., 2001: Viscous-plastic sea ice dynamics with the EVP model: Linearization issues. *J. Comput. Phys.*, **170**, 18–38, <https://doi.org/10.1006/jcph.2001.6710>.

- Krishfield, R. A., A. Proshutinsky, K. Tateyama, W. J. Williams, E. C. Carmack, F. A. McLaughlin, and M.-L. Timmermans, 2014: Deterioration of perennial sea ice in the Beaufort Gyre from 2003 to 2012 and its impact on the oceanic freshwater cycle. *J. Geophys. Res. Oceans*, **119**, 1271–1305, <https://doi.org/10.1002/2013JC008999>.
- Kwok, R., and J. Morison, 2017: Recent changes in Arctic sea ice and ocean circulation. *U.S. CLIVAR Variations Newsletter*, Vol. 15, No. 3, U.S. CLIVAR Project Office, Washington, DC, 1–6, <https://doi.org/10.5065/D6833QQP>.
- Large, W. G., and S. G. Yeager, 2009: The global climatology of an interannually varying air-sea flux data set. *Climate Dyn.*, **33**, 341–364, <https://doi.org/10.1007/s00382-008-0441-3>.
- Lique, C., H. L. Johnson, and P. E. D. Davis, 2015: On the interplay between the circulation in the surface and the intermediate layers of the Arctic Ocean. *J. Phys. Oceanogr.*, **45**, 1393–1409, <https://doi.org/10.1175/JPO-D-14-0183.1>.
- Manucharyan, G., and M. Spall, 2016: Wind-driven freshwater buildup and release in the Beaufort Gyre constrained by mesoscale eddies. *Geophys. Res. Lett.*, **43**, 273–282, <https://doi.org/10.1002/2015GL065957>.
- Marshall, J., J. Scott, and A. Proshutinsky, 2017: “Climate response functions” for the Arctic Ocean: A proposed coordinated modelling experiment. *Geosci. Model Dev.*, **10**, 2833–2848, <https://doi.org/10.5194/gmd-10-2833-2017>.
- Meneghello, G., J. Marshall, S. Cole, and M. L. Timmermans, 2017: Observational inferences of lateral eddy diffusivity in the halocline of the Beaufort Gyre. *Geophys. Res. Lett.*, **44**, 12 331–12 338, <https://doi.org/10.1002/2017GL075126>.
- , —, J. Campin, E. Doddridge, and M.-L. Timmermans, 2018a: The ice-ocean governor: Ice-ocean stress feedback limits Beaufort Gyre spin-up. *Geophys. Res. Lett.*, **45**, 11 293–11 299, <https://doi.org/10.1029/2018GL080171>.
- , —, M. Timmermans, and J. Scott, 2018b: Observations of seasonal upwelling and downwelling in the Beaufort Sea mediated by sea ice. *J. Phys. Oceanogr.*, **48**, 795–805, <https://doi.org/10.1175/JPO-D-17-0188.1>.
- Morison, J., R. Kwok, C. Peralta-Ferriz, M. Alkire, I. Rigor, R. Andersen, and M. Steele, 2012: Changing Arctic Ocean freshwater pathways. *Nature*, **481**, 66–70, <https://doi.org/10.1038/nature10705>.
- Parkinson, C., and W. Washington, 1979: A large-scale numerical model of sea ice. *J. Geophys. Res.*, **84**, 311–337, <https://doi.org/10.1029/JC084iC01p00311>.
- Petty, A., J. Hutchings, J. Richter-Menge, and M. Tschudi, 2016: Sea ice circulation around the Beaufort Gyre: The changing role of wind forcing and the sea ice state. *J. Geophys. Res. Oceans*, **121**, 3278–3296, <https://doi.org/10.1002/2015JC010903>.
- Proshutinsky, A., R. H. Bourke, and F. A. McLaughlin, 2002: The role of the Beaufort Gyre in Arctic climate variability: Seasonal to decadal climate scales. *Geophys. Res. Lett.*, **29**, 2100, <https://doi.org/10.1029/2002GL015847>.
- , and Coauthors, 2009: Beaufort Gyre freshwater reservoir: State and variability from observations. *J. Geophys. Res.*, **114**, C00A10, <https://doi.org/10.1029/2008JC005104>.
- , D. Dukhovskoy, M.-L. Timmermans, R. Krishfield, and J. Bamber, 2015: Arctic circulation regimes. *Philos. Trans. Roy. Soc.*, **373A**, 2052, <https://doi.org/10.1098/rsta.2014.0160>.
- Rabatel, M., P. Rampal, A. Carrassi, L. Bertino, and C. K. R. T. Jones, 2018: Impact of rheology on probabilistic forecasts of sea ice trajectories: Application for search and rescue operations in the Arctic. *Cryosphere*, **12**, 935–953, <https://doi.org/10.5194/tc-12-935-2018>.
- Rabe, B., and Coauthors, 2011: An assessment of Arctic Ocean freshwater content changes from the 1990s to the 2006–2008 period. *Deep-Sea Res. I*, **58**, 173–185, <https://doi.org/10.1016/j.dsr.2010.12.002>.
- Rampal, P., S. Bouillon, E. Ólason, and M. Morlighem, 2016: neXtSIM: A new Lagrangian sea ice model. *Cryosphere*, **10**, 1055–1073, <https://doi.org/10.5194/tc-10-1055-2016>.
- Roach, L. A., C. Horvat, S. M. Dean, and C. M. Bitz, 2018: An emergent sea ice floe size distribution in a global coupled ocean-sea ice model. *J. Geophys. Res. Oceans*, **123**, 4322–4337, <https://doi.org/10.1029/2017JC013692>.
- Spren, G., R. Kwok, and D. Menemenlis, 2011: Trends in Arctic sea ice drift and role of wind forcing: 1992–2009. *Geophys. Res. Lett.*, **38**, L19501, <https://doi.org/10.1029/2011GL048970>.
- Steele, M., R. Morley, and W. Ermold, 2001: PHC: A global ocean hydrography with a high-quality Arctic Ocean. *J. Climate*, **14**, 2079–2087, [https://doi.org/10.1175/1520-0442\(2001\)014<2079:PAGOHW>2.0.CO;2](https://doi.org/10.1175/1520-0442(2001)014<2079:PAGOHW>2.0.CO;2).
- Wang, Q., S. Danilov, and J. Schröter, 2008: Finite element ocean circulation model based on triangular prismatic elements, with application in studying the effect of vertical discretization. *J. Geophys. Res.*, **113**, C05015, <https://doi.org/10.1029/2007JC004482>.
- , —, D. Sidorenko, R. Timmermann, C. Wekerle, X. Wang, T. Jung, and J. Schröter, 2014: The Finite Element Sea Ice-Ocean Model (FESOM) v.1.4: Formulation of an ocean general circulation model. *Geosci. Model Dev.*, **7**, 663–693, <https://doi.org/10.5194/gmd-7-663-2014>.
- , —, T. Jung, L. Kaleschke, and A. Wernecke, 2016a: Sea ice leads in the Arctic Ocean: Model assessment, interannual variability and trends. *Geophys. Res. Lett.*, **43**, 7019–7027, <https://doi.org/10.1002/2016GL068696>.
- , and Coauthors, 2016b: An assessment of the Arctic Ocean in a suite of interannual CORE-II simulations. Part I: Sea ice and solid freshwater. *Ocean Modell.*, **99**, 110–132, <https://doi.org/10.1016/j.ocemod.2015.12.008>.
- , and Coauthors, 2016c: An assessment of the Arctic Ocean in a suite of interannual CORE-II simulations. Part II: Liquid freshwater. *Ocean Modell.*, **99**, 86–109, <https://doi.org/10.1016/j.ocemod.2015.12.009>.
- , C. Wekerle, S. Danilov, N. Koldunov, D. Sidorenko, D. Sein, B. Rabe, and T. Jung, 2018a: Arctic sea ice decline significantly contributed to the unprecedented liquid freshwater accumulation in the Beaufort Gyre of the Arctic Ocean. *Geophys. Res. Lett.*, **45**, 4956–4964, <https://doi.org/10.1029/2018GL077901>.
- , —, —, X. Wang, and T. Jung, 2018b: A 4.5 km resolution Arctic Ocean simulation with the global multi-resolution model FESOM 1.4. *Geosci. Model Dev.*, **11**, 1229–1255, <https://doi.org/10.5194/gmd-11-1229-2018>.
- Wekerle, C., Q. Wang, S. Danilov, T. Jung, and J. Schröter, 2013: The Canadian Arctic Archipelago throughflow in a multi-resolution global model: Model assessment and the driving mechanism of interannual variability. *J. Geophys. Res. Oceans*, **118**, 4525–4541, <https://doi.org/10.1002/jgrc.20330>.
- Yamamoto-Kawai, M., F. A. McLaughlin, E. C. Carmack, S. Nishino, K. Shimada, and N. Kurita, 2009: Surface freshening of the Canada Basin, 2003–2007: River runoff versus sea ice meltwater. *J. Geophys. Res.*, **114**, C00A05, <https://doi.org/10.1029/2008JC005000>.
- Yang, J., A. Proshutinsky, and X. Lin, 2016: Dynamics of an idealized Beaufort Gyre: 1. The effect of a small beta and lack of

- western boundaries. *J. Geophys. Res. Oceans*, **121**, 1249–1261, <https://doi.org/10.1002/2015JC011296>.
- Zhang, J., and Coauthors, 2016: The Beaufort Gyre intensification and stabilization: A model-observation synthesis. *J. Geophys. Res. Oceans*, **121**, 7933–7952, <https://doi.org/10.1002/2016JC012196>.
- Zhang, X., J. He, J. Zhang, I. Polyakov, R. Gerdes, J. Inoue, and P. Wu, 2013: Enhanced poleward moisture transport and amplified northern high-latitude wetting trend. *Nat. Climate Change*, **3**, 47–51, <https://doi.org/10.1038/nclimate1631>.
- Zhao, M., M.-L. Timmermans, S. Cole, R. Krishfield, and J. Toole, 2016: Evolution of the eddy fields in the Arctic Ocean's Canada Basin, 2005–2015. *Geophys. Res. Lett.*, **43**, 8106–8114, <https://doi.org/10.1002/2016GL069671>.
- Zhong, W., M. Steele, J. Zhang, and J. Zhao, 2018: Greater role of geostrophic currents in Ekman dynamics in the western Arctic Ocean as a mechanism for Beaufort Gyre stabilization. *J. Geophys. Res. Oceans*, **123**, 149–165, <https://doi.org/10.1002/2017JC013282>.